# A novel locally adaptive method for modeling the spatiotemporal dynamics of global electric power consumption based on DMSP-OLS nighttime stable light data

Ting Hu[a], Xin Huang[a,b,*]

[a] School of Remote Sensing and Information Engineering, Wuhan University, Wuhan 430079, PR China
[b] State Key Laboratory of Information Engineering in Surveying, Mapping and Remote Sensing, Wuhan University, Wuhan 430079, PR China

## HIGHLIGHTS

- A novel local-adaptive method was proposed to model global EPC at 1 km resolution.
- Multiple options were adopted to adaptively correct the NSL data.
- Various regression models were used to reflect the relationship between EPC and NSL.
- Our product showed higher spatiotemporal precision compared to the current one.
- The spatiotemporal dynamics of global electric power consumption were investigated.

## ARTICLE INFO

## ABSTRACT

Timely and reliable estimation of electricity power consumption (EPC) is essential to the rational deployment of electricity power resources. Nighttime stable light (NSL) data from the Defense Meteorological Satellite Program Operational Linescan System (DMSP-OLS) have the potential to model global 1-km gridded EPC. A processing chain to estimate EPC includes: (1) NSL data correction; and (2) regression model between EPC statistics and NSL data. For the global gridded EPC estimation, the current approach is to correct the global NSL image in a uniform manner and establish the linear relationships between NSL and EPC. However, the impacts of local socioeconomic inconsistencies on the NSL correction and model establishment are not fully considered. Therefore, in this paper, we propose a novel locally adaptive method for global EPC estimation. Firstly, we set up two options (with or without the correction) for each local area considering the global NSL image is not saturated everywhere. Secondly, three directions (forward, backward, or average) are alternatives for the inter-annual correction to remove the discontinuity effect of NSL data. Thirdly, four optional models (linear, logarithmic, exponential, or second-order polynomial) are adopted for the EPC estimation of each local area with different socioeconomic dynamic. Finally, the options for each step constitute all candidate processing chains, from which the optimal one is adaptively chosen for each local area based on the coefficient of determination. The results demonstrate that our product outperforms the existing one, at global, continental, and national scales. Particularly, the proportion of countries/districts with a high accuracy (MARE (mean of the absolute relative error) $\leq 10\%$) increases from 17.8% to 57.8% and the percentage of countries/districts with inaccurate results (MARE $> 50\%$) decreases sharply from 23.0% to 3.7%. This product can enhance the detailed understanding of the spatiotemporal dynamics of global EPC.

## 1. Introduction

Along with the tremendous development of the global economy, energy demand has continuously increased over the last century [1,2]. As an indispensable component of energy, electric power plays a vital role in numerous aspects of modern society, such as improving residential living standards [3], supporting industrial production [4], and promoting commercial transactions [5]. According to the World Bank [6], global electric power consumption (EPC) in 2014 was more than four times higher than that in 1971. In addition to the convenience

---

* Corresponding author at: School of Remote Sensing and Information Engineering, Wuhan University, Wuhan 430079, PR China.
  *E-mail address:* xhuang@whu.edu.cn (X. Huang).

brought by the massive increase of EPC, the world has also been burdened with accelerated global warming and air pollution due to the accompanying emission of greenhouse gases and other pollutants [7,8]. Therefore, accurate delineation of the spatiotemporal dynamics of global EPC is a critical prerequisite for investigating both the impacts of EPC and its interaction with the economy and the environment [9,10].

A wealth of research has investigated the spatiotemporal dynamics of EPC based on the EPC statistics published by related official organizations. For instance, AI-Garni et al. [11] adopted a regression model to forecast EPC in Eastern Saudi Arabia using weather data, global solar radiation, and population as variables. Egelioglu et al. [12] predicted annual EPC by multiple regression analyses of the historical economic databases and EPC statistics for Northern Cyprus. Shiu and Lam [13] examined the causal relationship between EPC and GDP in China by the error-correction model. Huang et al. [14] investigated the electric power supply and demand in China using the Grey-Markov forecasting model. Chujai et al. [15] forecasted the EPC at a household scale with different autoregressive models based on time-series EPC statistics. Cabral et al. [16] developed a spatiotemporal method that considers spatial correlations to predict the EPC in Brazil. These previous studies have been devoted to providing suggestions for governments or organizations. However, for the EPC statistics, the collection process is labor-intensive and time-consuming. Moreover, the EPC statistics are unable to reflect the internal spatial details within the administrative unit, which limits our understanding of the spatiotemporal dynamics of EPC at smaller scales [17,18]. Compared with the statistics for an entire administrative unit, gridding is a more realistic representation for the investigation of EPC at finer scales. Therefore, efficient methods to produce a spatially gridded representation of worldwide EPC are urgently needed, and it is worth attempting to adopt appropriate spatial gridded data as a proxy for modeling global EPC.

Satellite remotely sensed imagery has been proved to be a reliable way to support large-scale investigations in numerous fields, such as global solar radiation [19], land surface temperature [20], land use and land cover [21], and $CO_2$ emission [22]. The nighttime light (NTL) remote sensing imagery, such as that obtained by the Defense Meteorological Satellite Program's Operational Linescan System (DMSP-OLS) [23], has the potential for EPC estimation over large areas, because NTL can directly reflect the EPC caused by anthropogenic socioeconomic activities at night [24–27]. Elvidge et al. [28] verified the high log-log relation between the lit areas in DMSP-OLS data and EPC for 200 countries during 1994–1995. Similarly, Lo [29] modeled the logarithmic relationship between DMSP-OLS NTL and EPC for 35 Chinese cities for the year 1997. Amaral et al. [30] found that DMSP-OLS NTL was linearly correlated with the statistical EPC for 1999 in Brazilian Amazonia. Chand et al. [31] analyzed the linear relationship between the increase of EPC and the increase of NTL in the major cities and states of India during 1993–2002. Townsend and Bruce [32] reported a strong second-order polynomial relationship between DMSP-OLS NTL and EPC at the state level in Australia for 1997–2002. Letu et al. [33] estimated EPC in Japan and other Asian countries from saturated-corrected DMSP-OLS data, and found a strong linear correlation [34] between EPC and DMSP-OLS data in Japan. He et al. [35] respectively modeled double-log relationships for different economic regions of the Chinese Mainland from 1995 to 2008 at the county level. Ma et al. [36] attempted three models (linear, power-law, and exponential function) to quantify the relationships between EPC statistics and DMSP-OLS NTL for more than 200 cities in China during 1994–2009, and suggested that the best quantitative model type varies with the different socioeconomic patterns. Xie and Weng [37] explored the country-level relationship between EPC statistics and DMSP-OLS NTL by the logarithmic function. Jing et al. [38] adopted the linear model to correlate EPC with DMSP-OLS NTL data at the provincial level in China. By summarizing the existing literature, it can be found that different types of models have been utilized across different regions when using NTL to estimate EPC, due to the disparity of the social,

economic, and urban development status among the different regions.

With respect to the estimation of spatially gridded EPC, Zhao et al. [39] estimated the provincial-level EPC based on the DMSP-OLS and population data in China, and generated pixel-level EPC through disaggregation. Cao et al. [40] proposed a statistics-to-grid scaling down method for mapping gridded EPC in China based on the integration of DMSP-OLS data, population and gross domestic product (GDP). He et al. [41] modeled annual pixel-based EPC in Chinese Mainland with DMSP-OLS and normalized difference vegetation index (NDVI). Xie and Weng [42] estimated gridded EPC of China using DMSP-OLS data, population and enhanced vegetation index (EVI) considering the difference between urban cores and suburban areas. Pan and Li [43] generated 1-km EPC map in China with different vegetation indices and DMSP-OLS data. Most of the existing studies have focused on modeling at the national, regional, or city level, however, research at the global scale is scarce, due to its complexity. An exception and a notable example is the study of Shi et al. [44], where the original NTL images were first corrected worldwide using a uniform framework, and the world was then partitioned into 48 regions according to the geographic locations and socioeconomic levels. Finally, a linear model between the EPC statistics and corrected NTL data for each region was individually built to explore the gridded EPC. Nonetheless, this method does not fully consider the influence of the uniqueness of local socioeconomic development on the following three aspects in the EPC estimation.

(1) The saturation issue of NTL data: The relatively low radiometric resolution (6 bits) of the OLS sensor results in saturation in the NTL data [45], especially in the centers of large cities. All digital number (DN) values of these saturated pixels are 63, and hence, the disparity within the urban centers cannot be distinguished. In Shi et al. [44], a modified invariant region (MIR) method was globally adopted to reduce the saturated pixels. Nevertheless, saturated pixels are not ubiquitous worldwide, especially in underdeveloped areas. Saturation correction can result in distortion of these unsaturated pixels in suburban and rural areas [46], and reduce the contribution of saturated pixels to the EPC estimation [42]. Therefore, it is not appropriate to globally utilize a unified framework for saturation correction.

(2) The incomparability and discontinuity effect of NTL data: The original NTL images cannot be directly compared with each other, due to the lack of onboard calibration for the OLS sensor. Specifically, the DN values in the images obtained from the same satellite fluctuate abnormally in different years, and discrepancies occur in the images collected by different satellites for the same year [47]. Shi et al. [44] performed inter-annul correction in a forward direction for the whole world to eliminate the abnormal fluctuation (i.e., discontinuity effect) [43,44,48]. However, in addition to the forward direction, other approaches (e.g., backward, average) can also be considered for the correction, resulting in different corrected NTL data [49,50]. With inappropriately corrected NTL data, the reliability and accuracy of EPC estimation can also be affected. Therefore, it is not reasonable to apply the same approach (e.g., forward) for all the regions with diverse socioeconomic dynamics throughout the world.

(3) The estimation model between the EPC statistics and the corrected NTL data: Shi et al. [44] employed linear models for all the regions in the world. However, as indicated by the previous studies [35–38], the appropriate type of regression model can vary across areas, owing to the local socioeconomic diversity. Therefore, it is inappropriate to limit the model type to the linear one at the global scale.

To address the aforementioned research questions, we propose a novel locally adaptive method for modeling global EPC. Since the available EPC statistics across the globe are at the national level, the local scale in this study is set as the country/district level. Specifically,

for each country/district, two options (with or without correction) are first designed for saturation correction, and three optional directions (forward, backward, or average) are secondly considered for the inter-annual correction. Four alternative models (linear, logarithmic, exponential, or second-order polynomial functions) are then set up to reflect the possible relationships between the EPC and NTL data. Finally, the processing chain composed of the optimal options in the three aspects is adaptively selected for each country/district, to accommodate the local socioeconomic status.

The rest of this paper is organized as follows. Section 2 focuses on the data sources used in this study. Section 3 introduces the proposed locally adaptive selection method for global EPC mapping. The results and discussion are respectively presented in Sections 4 and 5. Finally, Section 6 sets out our main conclusions.

## 2. Data sources

The Version 4 global nighttime stable light (NSL) data of DMSP-OLS for 1992–2013 were obtained from the National Oceanic and Atmospheric Administration-National Geophysical Data Center (NOAA/NGDC) website (http://www.ngdc.noaa.gov/eog/dmsp.html). The NSL images were acquired by six satellites: F10 (1992–1994), F12 (1994–1999), F14 (1997–2003), F15 (2000–2007), F16 (2004–2009), and F18 (2010–2013), covering an area from −180 to 180 degrees in longitude and −65 to 75 degrees in latitude. The 34 annual NSL images over the 22 years are all in the 30 arc-second grid, with DN values ranging from 0 to 63. The global radiance-calibrated nighttime light (RCNL) image for 2006 was also downloaded from the same website for the intercalibration process of the NSL data.

In addition to the NSL data, we also downloaded the Version 4 Advanced Very High Resolution Radiometer (AVHRR) gridded daily normalized difference vegetation index (NDVI) dataset (https://doi.org/10.7289/V5PZ56R6) from the Google Earth Engine (GEE, http://earthengine.google.com/) to generate the annual mean NDVI composites worldwide, with a resolution of 0.05 arc degrees, for 1992–2013. The annual NSL, RCNL, and NDVI images were all resampled to the pixel size of 1 km on Mollweide projection. The EPC statistics for the countries/districts around the world were obtained from the World Bank Open Database (https://data.worldbank.org/), and the global continent and country boundary data were downloaded from the Version 2.8 Database of Global Administrative Areas (GADM, http://gadm.org/). Moreover, six scenes of Landsat 8 Operational Land Imager (OLI) images from the United States Geological Survey (USGS, https://earthexplorer.usgs.gov/) and the global Suomi National Polar-orbiting Partnership (NPP) Visible Infrared Imaging Radiometer Suite (VIIRS) Day/Night Band (DNB) data in 2013 were utilized to evaluate the performance of the NSL saturation correction. A brief description of the datasets used in this study is provided in Table 1.

## 3. Methodology

The proposed locally adaptive method for modeling global EPC consists of four main procedures: (1) decomposition of the global NSL images into national NSL data based on the national boundaries; (2)

sequential connection of all possible options in the NSL data correction (including the saturation correction and inter-annual correction) and EPC estimation to form all the candidate processing chains; (3) locally adaptive selection of the optimal processing chains to construct the global EPC; (4) evaluation of the accuracy of the global EPC and monitoring of the spatiotemporal dynamics of global EPC from 1992 to 2013 (Fig. 1).

### 3.1. NSL data correction (model steps 1–4)

Model step 1 (saturation correction): The fact that urban surfaces and vegetation are inversely correlated makes vegetation widely used for the saturation correction of NSL data. With the NSL data corrected by vegetation, this can de-saturate the pixels in the core urban areas. However, it may also result in distortion for those unsaturated pixels in suburban and rural areas [46]. Therefore, the first step in correcting the NSL data was to determine whether saturation correction should be performed for each region. If saturation correction was needed, we adopted the vegetation adjusted normalized urban index (VANUI) [51] to alleviate the saturation effect of NSL by the association of the NDVI:

$$VANUI = (1 - NDVI) \times NSL \tag{1}$$

where NDVI is the annual mean NDVI derived from daily AVHRR-NDVI. Details can be found in Zhang et al. [51]. If saturation correction was not necessary, the original NSL DN values were retained. Therefore, there are two options in this step, i.e., whether to conduct the saturation correction or not.

Model step 2 (intercalibration): Another issue of NSL data is the inconsistency of different NSL images, whether they are from the same year or the same satellite. The 34 global NSL images for 1992–2013 needed to be intercalibrated by the invariant region (IR) method, under the assumption that the relationship built in the invariant region can be extended to broader areas [43,52]. Following Shi et al. [44], Japan was selected as the IR due to its relatively-stable socioeconomic status during the study period and wide range of NSL DN values [44,53]. The power regression model was then utilized to build the relationship between the reference data and the NSL images to be calibrated. For the original NSL images, the RCNL image from 2006 was chosen as the reference, due to its wide range of DN values [54]. As for the saturation-corrected images, the VANUI image derived from the F16 satellite in 2006 was selected as the reference. The relationship in Japan was then established as:

$$DN_{Jap}^{Img} = a \times \left(DN_{Jap}^{Ref}\right)^b \tag{2}$$

where $DN_{Jap}^{Img}$ denotes the DN value of the image to be intercalibrated in Japan; $DN_{Jap}^{Ref}$ stands for the DN value of the reference image in Japan; and a and b are the coefficients of the model, which were determined by regression analysis. In this way, the global NSL and VANUI images could be respectively intercalibrated using their corresponding coefficients.

Model step 3 (intra-annual composition): To take full advantage of the two images from the same year [55], an intra-annual composition of the NSL (or VANUI) images was conducted as follows:

**Table 1**
Description of the datasets.

| Data | Data description | Source |
|---|---|---|
| NSL | Annual nighttime stable light data for 1992–2013 | NOAA/NGDC |
| RCNL | Global radiance-calibrated nighttime light data for 2006 | NOAA/NGDC |
| NDVI | Annual mean NDVI composites from 1992 to 2013 | AVHRR/GEE |
| Landsat 8 OLI | Six images covering six cities from three countries of various economic levels | USGS |
| VIIRS/DNB | Visible Infrared Imaging Radiometer Suite Day/Night Band data in 2013 | NOAA/NGDC |
| EPC | Annual EPC statistics for 1992–2013 | World Bank Open Database |
| Boundaries | Shapefile of global continents and countries in 2013 | Global Administrative Areas |
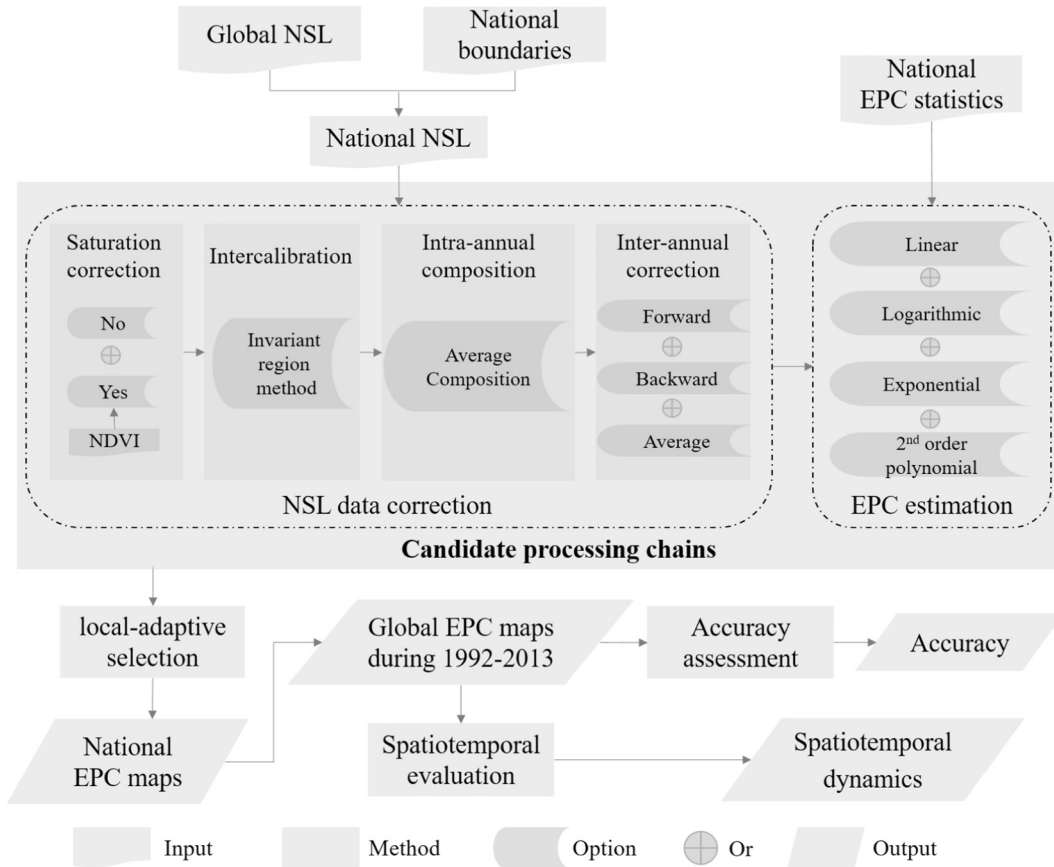
Fig. 1. Flowchart of the proposed methodology.

$$DN_{(k,i)}^{intra} = \begin{cases} 0 & DN_{(k,i)}^1 = 0 \\ 0 & DN_{(k,i)}^2 = 0 \\ (DN_{(k,i)}^1 + DN_{(k,i)}^2)/2 & otherwise \end{cases} \quad (3)$$

where $DN_{(k,i)}^{intra}$ is the DN value of pixel $i$ after the intra-annual composition in the year $k$, $DN_{(k,i)}^1$ and $DN_{(k,i)}^2$ respectively denote the DN values of pixel $i$ from two intercalibrated NSL (or VANUI) images in the year $k$, and $k$ stands for the number of years in 1994 and 1997–2007.

Model step 4 (inter-annual correction): The discontinuity effect still existed among the annual images after the correction using Eq. (3). To erase the abnormal fluctuations, an inter-annual correction was further performed using Eq. (4), according to [43,44,48], by assuming that the DN value of each lit pixel would not decrease over time with the rapid development of the global economy.

$$DN_{(k,i)}^{inter} = \begin{cases} 0 & DN_{(k-1,i)} = 0 \\ DN_{(k-1,i)} & DN_{(k+1,i)} > 0 \ and \ DN_{(k-1,i)} > DN_{(k,i)} \\ DN_{(k+1,i)} & otherwise \end{cases} \quad (4)$$

where $DN_{(k,i)}^{inter}$ is the DN value of pixel $i$ after inter-annual correction in year $k$; $DN_{(k-1,i)}$, $DN_{(k,i)}$, and $DN_{(k+1,i)}$ are the DN values of pixel $i$ from the intra-annual composited NSL (or VANUI) images in the years $k-1$, $k$, and $k + 1$; and $k$ is the number of years from 1992 to 2013. However, please note the base year is not explicitly mentioned in Eq. (4). Different options of base year would result in different inter-annual-corrected NSL (or VANUI) data. When the base year was set to 1992, it meant that the $k$ in Eq. (4) started from 1992, and thus the inter-annual correction was performed in a forward direction; likewise, when the base year was set to 2013, it denoted that the $k$ in Eq. (4) started from 2013 and, in this way, the inter-annual correction was conducted in a backward direction. Another possible option was the average of the forward and backward directions, which can smooth the bias of each

direction [50]. In total, there are three options in the step of inter-annual correction in our model.

At this stage, the NSL data correction included six different combinations, related to the consideration of the vegetation index for mitigating the NSL saturation (with or without NDVI) and the mode of inter-annual correction (forward, backward or average).

3.2. EPC estimation (model step 5)

The process of global urbanization actually varies across regions, and is a comprehensive reflection of the local social and economic status. Various types of relationships between EPC (an endogenous urbanization variable) and NSL likely indicate the diverse underlying local socioeconomic patterns [36]. To portray the possible correlations between EPC and NSL data in various countries with different socioeconomic patterns of spatiotemporal dynamics, in our method, four different types of regression models, i.e., linear, logarithmic, exponential, and second-order polynomial functions, can be chosen.

(1) The linear model was used to represent the status where the EPC response was proportional to the NSL.
(2) The logarithmic model with a convex shape assumed that the EPC showed a gradually declining response rate to the increase of NSL, implying that the EPC would reach saturation with the increase of nighttime lights.
(3) The exponential model with a concave shape represented a gradually increasing response rate of EPC to the rise of NSL.
(4) The second-order polynomial model has the potential to represent both the increasing and decreasing response rate of EPC to the rise of NSL, which is associated with the coefficient of the quadratic term. When the coefficient is positive, the model portrays an increasing response rate of EPC to the increase of NSL, and the

negative coefficient denotes a decreasing response rate to the rise of NSL. This model has been used to estimate EPC in Australia [32], and thus it was also selected as an option in this study.

As suggested in [40–44], the estimation of gridded EPC was based on a hypothesis that, for each pixel within a country/district, the relationship between the DN value of the corrected NSL and EPC value is consistent. In this research, we represented this relationship as:

$$\text{EPC}_{(i,j)} = \boldsymbol{F}\ (\text{NSL}_{(i,j)}) \tag{5}$$

where $\boldsymbol{F}$ is one of the four relationships defined in our method, $\text{NSL}_{(i,j)}$ denotes the DN value of pixel $i$ in country $j$ in the corrected NSL data, and $\text{EPC}_{(i,j)}$ stands for the estimated EPC value of pixel $i$ in country $j$. The four candidate types of $\boldsymbol{F}$ functions are as follows:

Linear: $\text{EPC}_{(i,j)} = p_1 \times \text{NSL}_{(i,j)}$ (6)

Logarithmic: $\text{EPC}_{(i,j)} = p_2 * \ln(\text{NSL}_{(i,j)} + 1)$ (7)

Exponential: $\text{EPC}_{(i,j)} = p_3 \times (e^{\text{NSL}_{(i,j)}} - 1)$ (8)

$2\text{nd} - \text{order\ polynomial}: \text{EPC}_{(i,j)} = p_4 * \text{NSL}_{(i,j)}^2 + q_4 * \text{NSL}_{(i,j)}$ (9)

where $p_i(i = 1, 2, 3, 4)$ as well as $q_4$ are coefficients of the models.

By summing up the DN values of all the pixels belonging to country $j$, country-level EPC values can then be obtained as follows:

Linear: $\text{EPC}_j^{stat} = p_1 \times \sum_{i=1}^{N_j} \text{NSL}_{(i,j)}$ (10)

Logarithmic: $\text{EPC}_j^{stat} = p_2 * \sum_{i=1}^{N_j} \ln(\text{NSL}_{(i,j)} + 1)$ (11)

Exponential: $\text{EPC}_j^{stat} = p_3 \times \sum_{i=1}^{N_j} (e^{\text{NSL}_{(i,j)}} - 1)$ (12)

$2\text{nd} - \text{order\ polynomial}: \text{EPC}_j^{stat} = p_4 * \sum_{i=1}^{N_j} \text{NSL}_{(i,j)}^2$
$+ q_4 * \sum_{i=1}^{N_j} \text{NSL}_{(i,j)}$ (13)

where $N_j$ is the number of pixels in country $j$, and $\text{EPC}_j^{stat}$ is the statistical EPC for country $j$. Using the least-squares method, the coefficients in Eqs. (10)–(13) for each country/district could be respectively solved based on the EPC statistics and the NSL data from 1992 to 2013.

To summarize, the six options in NSL correction and four options in regression model yielded 24 candidate processing chains for the EPC estimation of each country/district.

### 3.3. Locally adaptive EPC estimation (model step 6)

This step involves adaptively selecting the most suitable strategy for each country/district from the 24 candidate processing chains. The coefficient of determination ($R^2$), a measure of goodness-of-fit, is widely used to assess the performance of a regression model [36,56]. Therefore, the processing chain with the highest $R^2$ was selected as the optimal one for the EPC estimation in each country/district. In particular, please note that the EPC statistics from the World Bank Open Database for 1992–2013 are incomplete. To obtain more reliable estimations, the countries with less than 5 years' observational data [36] were not included in the modeling for the EPC estimation. The models of these countries were substituted by those of countries/districts with sufficient statistics in the same region, as suggested by Shi et al. [44]. In this way, the global EPC maps at a 1-km resolution from 1992 to 2013 could be constructed.

### 3.4. Spatiotemporal dynamics of EPC (model step 7)

The 1-km global EPC maps for 1992–2013 provide us with the potential to portray the spatiotemporal dynamics of global EPC with fine spatial details. The gridded EPC was aggregated to the Level-1 subdivision unit in the Global Administrative Areas Dataset (GADM). For

example, the Level-1 subdivision units in China and the United States are the provincial and state levels, and thus we hereafter refer to the Level-1 unit in GADM as the provincial/state level. We adopted the global and local Moran's $I$ indices to depict the spatial patterns of EPC across the world. The global Moran's $I$ index [57] is an overall measure of spatial autocorrelation, with the value ranging from $-1$ to 1. A positive value indicates the level of similarity, while a negative values denotes the degree of difference. The global Moran's $I$ index is formulated as:

$$I = \frac{N \sum_i \sum_j w_{ij} (x_i - \bar{x})(x_j - \bar{x})}{\sum_i \sum_j w_{ij} \sum_i (x_i - \bar{x})^2} \tag{14}$$

where $N$ is the number of provinces/states, $w_{ij}$ is the matrix of spatial weight of the $i$th and $j$th provinces/states based on the Queen's contiguity, $x_i$ and $x_j$ refer to the total EPC for the $i$th and $j$th provinces/states, and $\bar{x}$ denotes the average EPC of all the provinces/states.

The local Moran's $I$ index indicates the degree of spatial autocorrelation between each sample and its neighbors. The index is calculated as [58]:

$$I_i = \frac{(x_i - \bar{x})}{s_i^2} \sum_{j, j \neq i} [w_{ij}(x_j - \bar{x})] \tag{15}$$

with $s_i^2 = \frac{\sum_{j, j \neq i}(x_j - \bar{x})^2}{N - 1} - \bar{x}^2$. It can be applied to describe four types of local spatial autocorrelation: (1) a High-High cluster (a high value surrounded by high values); (2) a Low-Low cluster (a low value surrounded by low values); (3) a High-Low cluster (a high value surrounded by low values); and (4) a Low-High cluster (a low value surrounded by high values).

According to He et al. [35], the *SLOPE* index was used to examine the variation trends of the provincial EPC from 1992 to 2013:

$$SLOPE_i = \frac{n \sum_{k=1}^{n} (y_k EPC_{i\_k}) - \sum_{k=1}^{n} y_k \sum_{k=1}^{n} EPC_{i\_k}}{n \sum_{k=1}^{n} y_k^2 - \left(\sum_{k=1}^{n} y_k\right)^2} \tag{16}$$

where $n$ is the number of years (i.e., 22), $y_k$ stands for the $k$th year from 1 to 22, and $EPC_{i\_k}$ is the total EPC in the $i$th province of the $k$th year. A positive value indicates an increasing trend, whereas a negative one indicates a decreasing tendency. The *SLOPE* index for each province/state was then divided into five grades using the Natural Breaks (Jenks) method, i.e., slow, relatively slow, moderate, relatively rapid, and rapid growth.

## 4. Results

### 4.1. Evaluation of the NSL data correction

#### 4.1.1. The saturation correction

To clearly show the effects of the saturation correction on the NSL data for areas with different socioeconomic levels, we visually compared the original NSL with saturation-corrected (VANUI) images for six cities in 2013, using the 30-m resolution Landsat 8 OLI images and the VIIRS/DNB data as the reference to show the urban regions (Fig. 2). Afghanistan, China, and the United States were selected as representative countries, considering their different development levels. Within each country, two cities were further chosen to represent the different urbanization levels. The original NSL images are displayed in Fig. 2(c), and the pixels with DN values of 63 (saturated pixels) are shown in Fig. 2(e) for each city. It can be seen that the saturation effect exists in Kabul (Afghanistan), Beijing (China), and Los Angeles (United States). However, the less-developed cities (Gardze, Ya'an, and Moore) have no saturated pixels.

For the cities where saturation can be observed (Kabul, Beijing, and Los Angeles), each VANUI image (Fig. 2(d)) shows a more similar pattern to the Landsat 8 images and the VIIRS data (Fig. 2(a)-(b)) than the NSL images (Fig. 2(c)), due to the improved inter-urban variability
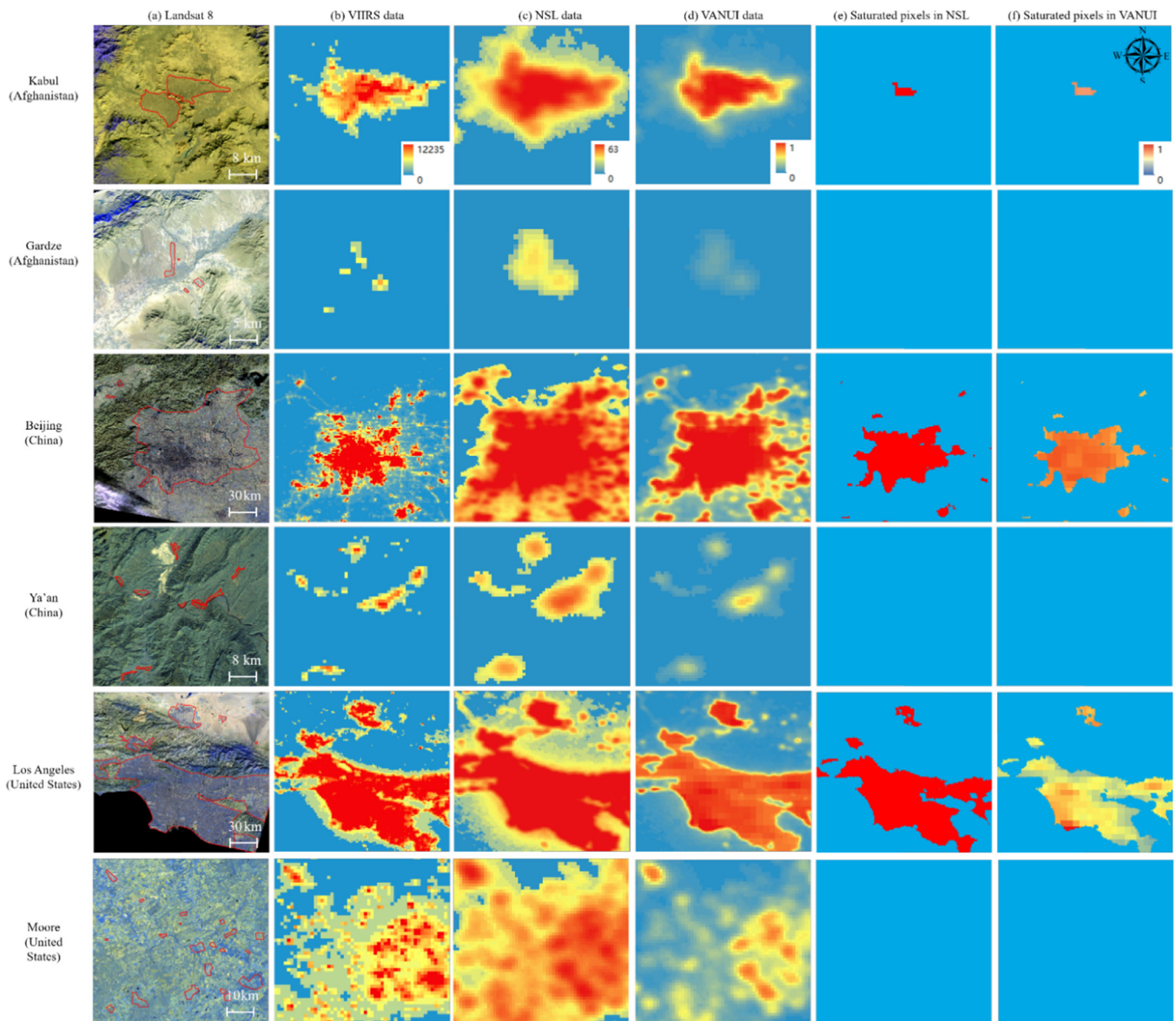
**Fig. 2.** Comparison between the original NSL data and the VANUI data for the selected cities in reference to: (a) Landsat 8 OLI images (R: 7, G: 6, B: 5) in 2013 and (b) VIIRS data in Dec. 2013; (c) NSL data with all values; (d) VANUI data with all values; (e) NSL data with saturated pixels highlighted; and (f) VANUI data with saturated pixels highlighted.

and the clearer transition of urban-suburban areas. The different VANUI values for saturated pixels were further displayed in Fig. 2(f), and it can be seen that the difference in the urban centers are clearly improved when compared with Fig. 2(e). In other words, the saturation issue in the urban centers can be effectively corrected in these cities using the vegetation index. Nevertheless, on the other hand, for the cities without saturated pixels (e.g., Gardze, Ya'an, and Moore), the information of the VANUI data (Fig. 2(d)) is not appropriate to represent the urban patterns, since it can result in distortion to the true representation of human nighttime lights, compared to the NSL data, especially in the suburbs and rural areas. These observations further prove that nationwide saturation correction is not necessarily appropriate. Therefore, it is reasonable to set up two options in the step of NSL saturation correction, and the optimal option should be chosen by locally adaptive selection, according to the $R^2$ of the regression model, for a more accurate EPC estimation.

### 4.1.2. The inter-annual correction

Inter-annual correction is performed to remove the abnormal fluctuations in the annual images after the intra-annual composition. As previously mentioned, different directions of inter-annual correction can lead to different corrected NSL data, as well as different EPC estimations. Fig. 3 displays the sums of the corrected NSL data related to different directions (original, forward, backward, and average) for four countries (Bangladesh, Algeria, Brazil, and Australia) with distinct geographical locations and development levels. Here, the original curve denotes the sum of nighttime lights without inter-annual correction. It can be clearly observed that strong random fluctuations in the inter-annual variation exist in the original curves of each country, demonstrating the need for inter-annual correction. It can also be seen that the discontinuity effect can be effectively suppressed, no matter which direction is used for the inter-annual correction. More consistent time-series NSL data would assist with the reliability of the subsequent EPC estimation [43,44,48].

To further explore the influence of the inter-annual correction direction on the EPC estimation, we employed four candidate models to establish the relationships between the EPC statistics and the four different corrected NSL results, respectively, for comparison. Please kindly
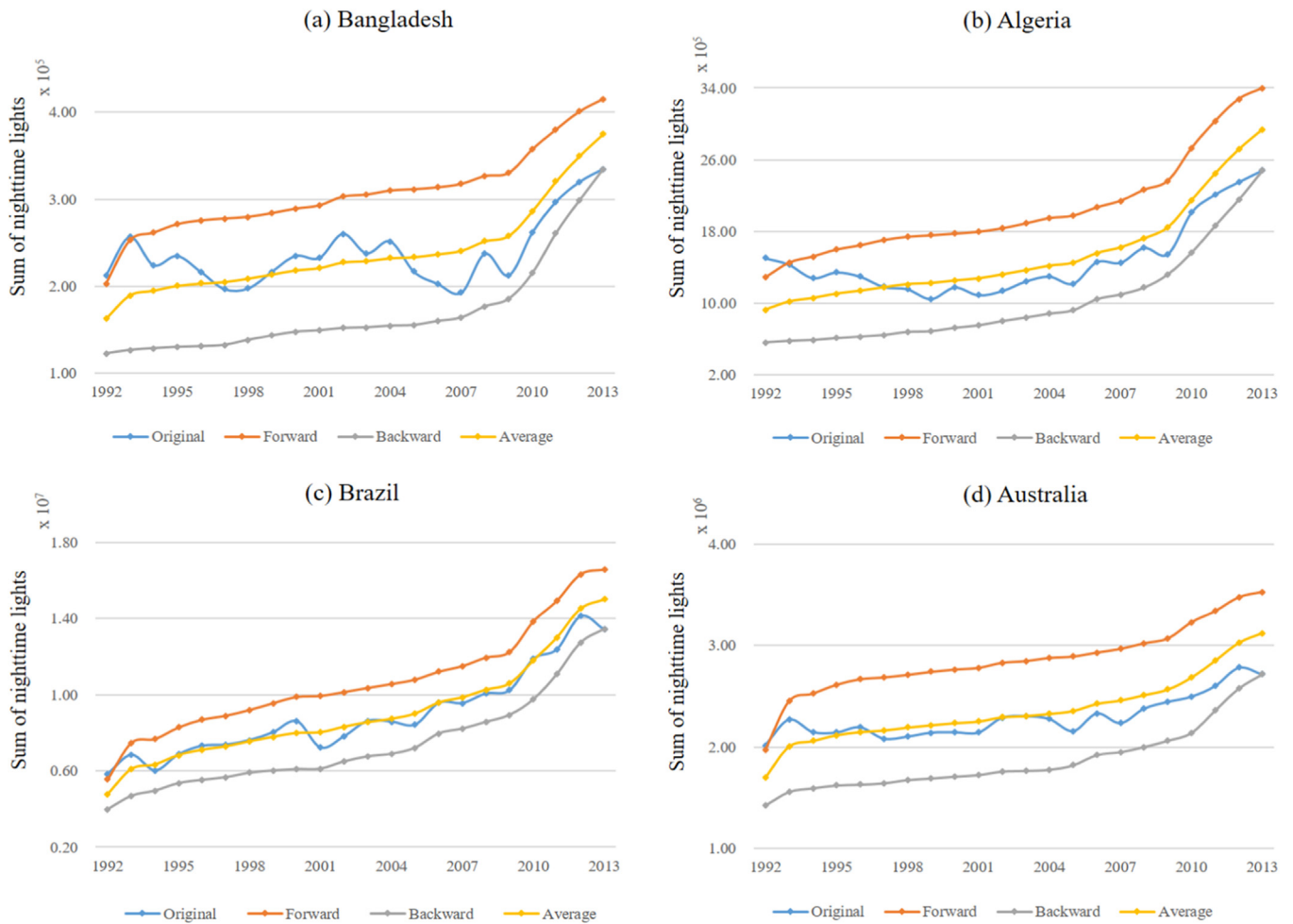
**Fig. 3.** Corrected NSL results with different directions of inter-annual correction for the four selected countries.

**Table 2**
The $R^2$ values of models based on the corrected NSL data with different directions (the optimal direction for each country and each regression model has been underlined).

| | Bangladesh | | | | Algeria | | | |
|---|---|---|---|---|---|---|---|---|
| | Original | Forward | Backward | Average | Original | Forward | Backward | Average |
| Linear | 0.2666* | 0.4473* | <u>0.7067*</u> | 0.5686* | 0.7095* | 0.9014* | 0.8063* | <u>0.9521*</u> |
| Logarithmic | 0.2219* | 0.5760* | <u>0.7243*</u> | 0.6310* | 0.7185* | 0.9356* | <u>0.9651*</u> | 0.9607* |
| Exponential | 0.0962 | 0.1735* | <u>0.6779*</u> | 0.5259* | 0.1451 | 0.5983* | 0.2590* | <u>0.8881*</u> |
| 2nd-order | 0.2404* | 0.3594* | <u>0.5140*</u> | 0.4929* | 0.6309* | 0.6578* | 0.7654* | <u>0.7841*</u> |
| | Brazil | | | | Australia | | | |
| | Original | Forward | Backward | Average | Original | Forward | Backward | Average |
| Linear | 0.9014* | <u>0.9340*</u> | 0.8784* | 0.9282* | 0.5355* | <u>0.7885*</u> | 0.5444* | 0.7524* |
| Logarithmic | 0.9451* | 0.9467* | 0.9512* | <u>0.9553*</u> | 0.5646* | <u>0.7766*</u> | 0.4552* | 0.7093* |
| Exponential | 0.3950* | <u>0.8812*</u> | 0.5198* | 0.8223* | 0.1093* | 0.3945* | 0.1439* | <u>0.5173*</u> |
| 2nd-order | 0.9437* | <u>0.9561*</u> | 0.7830* | 0.8974* | 0.5871* | <u>0.8145*</u> | 0.5111* | 0.6882* |

Note: * denotes $P < 0.05$.

note that for each regression model, the $R^2$ of each country varies with the correction direction (Table 2). For instance, when using the linear model, the highest $R^2$ value appears in the backward direction for Bangladesh, but the optimal $R^2$ value corresponds to the average direction for Algeria. These results imply that it is rational to adopt different options in the correction direction of NSL data. In this way, the optimal correction direction for EPC estimation can be locally determined.

### 4.2. Evaluation of the EPC estimation

#### 4.2.1. Different regression models

To explore the impact of different regression models on the EPC estimation, 8 countries are selected as representatives due to their different locations and socioeconomic levels, and Table 3 lists the $R^2$ values of the four candidate regression models. For each country, four models were established based on the same corrected NSL data and EPC

**Table 3**
The $R^2$ values of different regression models (the optimal model for each country has been underlined).

|  | Mexico | Pakistan | Yemen | Portugal | Dominican Republic | The Congo | Brazil | Australia |
|---|---|---|---|---|---|---|---|---|
| Linear | 0.8773[*] | 0.8996[*] | 0.9101[*] | 0.1767[*] | 0.8137[*] | 0.3657[*] | 0.9531[*] | 0.8258[*] |
| Logarithmic | 0.8637[*] | 0.8172[*] | 0.9317[*] | 0.8404[*] | 0.7702[*] | 0.1278[*] | 0.8756[*] | 0.6816[*] |
| Exponential | 0.8201[*] | 0.6579[*] | 0.8572[*] | 0.3413[*] | 0.8415[*] | 0.5454[*] | 0.9456[*] | 0.7952[*] |
| 2nd-order polynomial | 0.8046[*] | 0.5897[*] | 0.8954[*] | 0.5191[*] | 0.4754[*] | 0.2814[*] | 0.9634[*] | 0.8372[*] |

Note: [*] $P < 0.05$.

statistics. In this way, the difference of their $R^2$ values only originates from the regression models. It can be found that the linear models outperform the others in terms of $R^2$ values for Mexico and Pakistan, yet, in Yemen and Portugal, the logarithmic models achieve the highest $R^2$ values. The models with the highest $R^2$ values for the Dominican Republic and the Congo are the exponential ones, and with regard to Brazil and Australia, the highest $R^2$ values appear in the second-order polynomial models. In addition, significant differences in $R^2$ values can be observed among the four models of several countries, e.g., Portugal and Pakistan, showing that improper choice of regression model can substantially affect the accuracy and reliability of the EPC estimation. Therefore, it is necessary to consider different regression models, and to select the most suitable one to construct the estimation model, due to the socioeconomic variations among countries.

### 4.2.2. The optimal processing chains

Different options, associated with saturation correction, inter-annual correction, and the regression model, constitute a series of processing chains for the EPC estimation. We numbered all 24 processing chains, and show the optimal one for each country/district in the world in Fig. 4. The specific meaning of each processing chain is listed in Table 4, where, for instance, 'Yes' + 'Forward' + 'Linear' stands for a processing chain consisting of three options: saturation correction using NDVI, the forward inter-annual correction, and the linear regression model. The global EPC maps from 1992 to 2013, generated by the proposed locally adaptive method, are presented in Fig. 5. Four sites are selected as representatives to display the details of our generated EPC maps. It can be observed that Europe, Asia, and North America

consumed more electricity during this period, compared with the other regions in the world.

## 5. Discussion

### 5.1. Comparison with existing global products

Shi et al. [44] modeled 1-km resolution global EPC maps from 1992 to 2013 by dividing the world into a series of regions, with a linear regression model for each region (hereafter referred to as Shi's product). Here we compare our estimated global EPC maps with Shi's product at global, continental, and national levels, respectively, based on the country-level statistics.

### 5.1.1. Comparison at the global level

For each year during 1992–2013, we calculated the sum of the statistics for each country/district as the global total statistics, and compared this with our results. In addition to the $R^2$, we also adopted the relative error (RE) to assess the accuracy:

$$RE = \frac{\hat{y} - y}{y} \times 100\%$$

(17)

where $y$ is the statistical EPC value, and $\hat{y}$ stands for the estimated EPC. From Table 5, we can observe that nearly all the $R^2$ values of our product are larger than those of Shi's product, and the average $R^2$ value (0.998) is higher than that of Shi's product (0.996), with a significant difference captured by the ANOVA test [59] ($p$-value = 0.006). In terms of the mean of the absolute RE (hereafter referred to as MARE), our
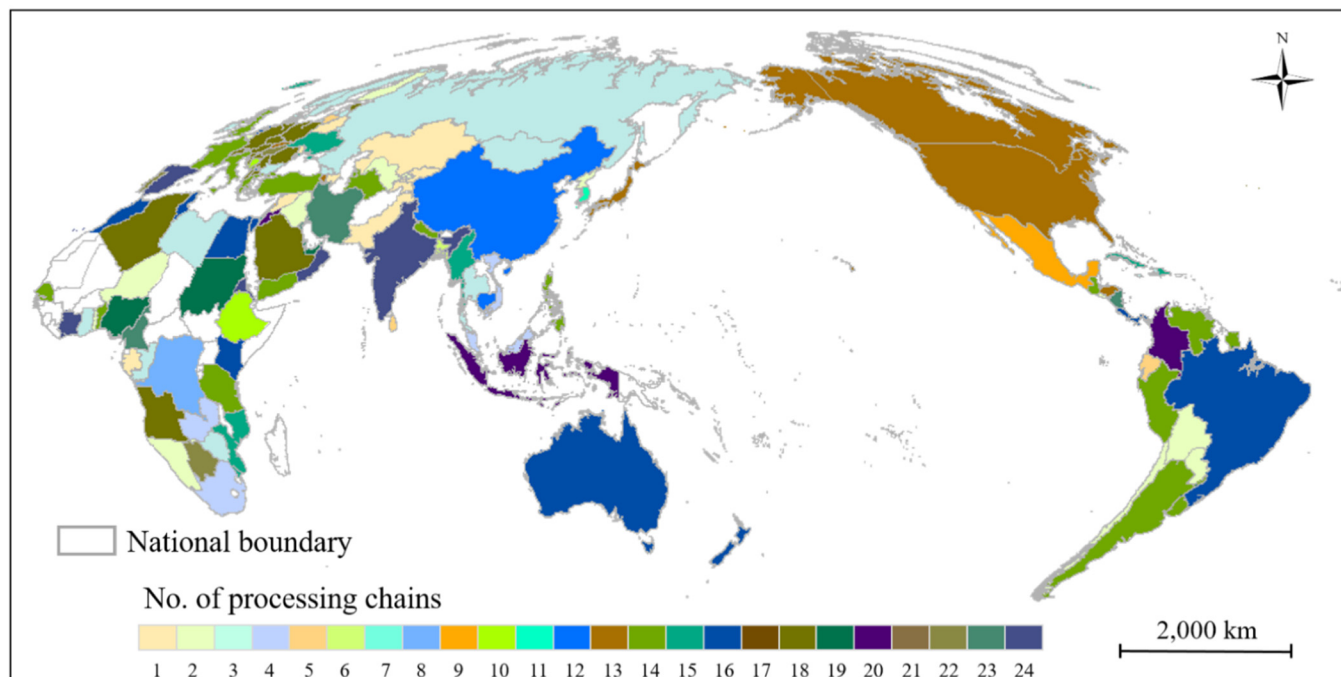


**Fig. 4.** The optimal processing chains for the EPC estimation of countries/districts in the world.

**Table 4**
The specific meaning of each processing chain.

| Combinations of options | No. | Combinations of options | No. | Combinations of options | No. |
|---|---|---|---|---|---|
| 'No' + 'Forward' + 'Linear' | 1 | 'No' + 'Average' + 'Linear' | 9 | 'Yes' + 'Backward' + 'Linear' | 17 |
| 'No' + 'Forward' + 'Logarithmic' | 2 | 'No' + 'Average' + 'Logarithmic' | 10 | 'Yes' + 'Backward' + 'Logarithmic' | 18 |
| 'No' + 'Forward' + 'Exponential' | 3 | 'No' + 'Average' + 'Exponential' | 11 | 'Yes' + 'Backward' + 'Exponential' | 19 |
| 'No' + 'Forward' + 'Polynomial' | 4 | 'No' + 'Average' + 'Polynomial' | 12 | 'Yes' + 'Backward' + 'Polynomial' | 20 |
| 'No' + 'Backward' + 'Linear' | 5 | 'Yes' + 'Forward' + 'Linear' | 13 | 'Yes' + 'Average' + 'Linear' | 21 |
| 'No' + 'Backward' + 'Logarithmic' | 6 | 'Yes' + 'Forward' + 'Logarithmic' | 14 | 'Yes' + 'Average' + 'Logarithmic' | 22 |
| 'No' + 'Backward' + 'Exponential' | 7 | 'Yes' + 'Forward' + 'Exponential' | 15 | 'Yes' + 'Average' + 'Exponential' | 23 |
| 'No' + 'Backward' + 'Polynomial' | 8 | 'Yes' + 'Forward' + 'Polynomial' | 16 | 'Yes' + 'Average' + 'Polynomial' | 24 |

product (3.011%) also outperforms Shi's product (3.338%).

### 5.1.2. Comparison at the continental level

Fig. 6 displays the RE values per year in each continent, except for Antarctica. It can be found that the curves of the two products are similar to each other in all six continents. However, the RE values of our results are closer to 0, in more cases. To compare the two products more clearly, the MARE values were further generated for each continent (Table 6). It can be seen that our product performs better than Shi's product for all the continents, by 0.5–2.5%. Significant differences can
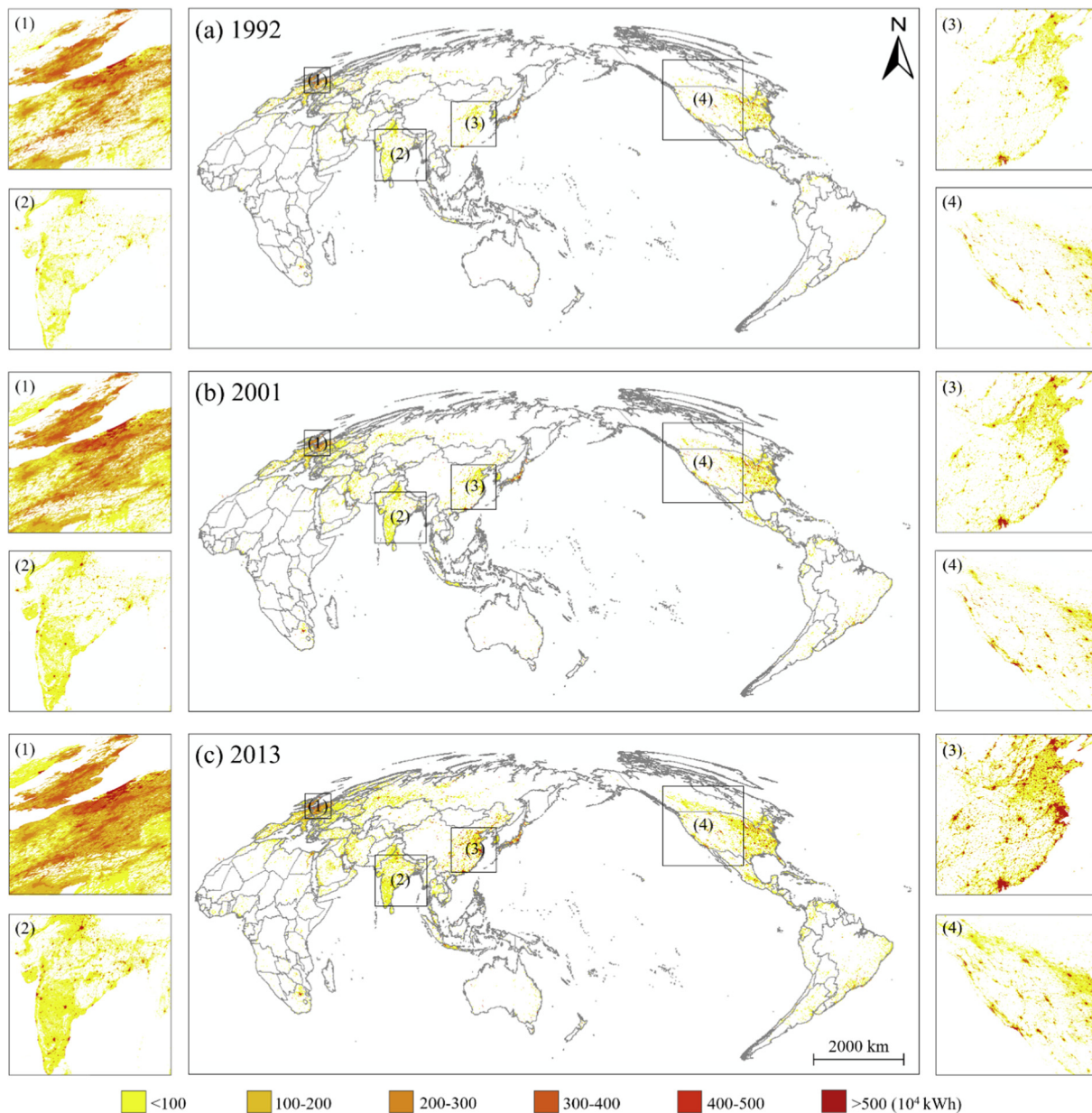


**Fig. 5.** The estimated global EPC maps in Mollweide projection for (a) 1992, (b) 2001, and (c) 2013 by utilizing the proposed locally adaptive method. Four sites, i.e., (1) Europe, (2) India, (3) China, and (4) the United States, are selected as examples.

**Table 5**
Accuracy assessment of the estimated global EPC from 1992 to 2013.

| Year | Ours | | | | Shi's product | | |
|---|---|---|---|---|---|---|---|
| | Statistical EPC ($10^8$ kWh) | Estimated EPC ($10^8$ kWh) | RE (%) | $R^2$ | Estimated EPC ($10^8$ kWh) | RE (%) | $R^2$ |
| 1992 | 109,092 | 92,590 | −15.127 | 0.988 | 90,833 | −16.738 | 0.993 |
| 1993 | 111,023 | 107,543 | −3.134 | 0.995 | 109,445 | −1.421 | 0.994 |
| 1994 | 113,893 | 111,966 | −1.691 | 0.997 | 114,700 | 0.709 | 0.995 |
| 1995 | 117,828 | 117,868 | 0.034 | 0.998 | 121,860 | 3.422 | 0.996 |
| 1996 | 121,649 | 119,883 | −1.452 | 0.998 | 125,179 | 2.902 | 0.996 |
| 1997 | 124,595 | 122,958 | −1.314 | 0.998 | 128,045 | 2.769 | 0.996 |
| 1998 | 127,543 | 125,699 | −1.446 | 0.998 | 130,974 | 2.690 | 0.996 |
| 1999 | 131,083 | 128,676 | −1.836 | 0.998 | 134,446 | 2.566 | 0.996 |
| 2000 | 137,041 | 133,164 | −2.829 | 0.998 | 138,337 | 0.945 | 0.997 |
| 2001 | 138,421 | 135,673 | −1.985 | 0.998 | 140,471 | 1.481 | 0.997 |
| 2002 | 143,396 | 140,424 | −2.073 | 0.997 | 144,914 | 1.059 | 0.997 |
| 2003 | 149,081 | 149,531 | 0.302 | 0.999 | 149,735 | 0.439 | 0.998 |
| 2004 | 155,690 | 155,179 | −0.329 | 0.999 | 154,163 | −0.981 | 0.998 |
| 2005 | 162,499 | 157,813 | −2.882 | 1.000 | 156,291 | −3.821 | 0.998 |
| 2006 | 169,363 | 162,549 | −4.023 | 1.000 | 160,648 | −5.146 | 0.998 |
| 2007 | 177,123 | 167,192 | −5.607 | 0.999 | 164,001 | −7.408 | 0.997 |
| 2008 | 180,772 | 173,013 | −4.290 | 0.999 | 167,580 | −7.298 | 0.997 |
| 2009 | 179,920 | 178,479 | −0.807 | 0.998 | 174,017 | −3.281 | 0.996 |
| 2010 | 192,862 | 192,585 | −0.144 | 0.999 | 190,823 | −1.057 | 0.996 |
| 2011 | 199,393 | 204,344 | 2.483 | 0.999 | 202,524 | 1.570 | 0.995 |
| 2012 | 203,815 | 213,278 | 4.643 | 0.999 | 210,287 | 3.176 | 0.995 |
| 2013 | 210,256 | 226,689 | 7.815 | 1.000 | 215,618 | 2.550 | 0.995 |
| Average $R^2$ | – | – | – | 0.998 | – | – | 0.996 |
| MARE | – | – | 3.011 | – | – | 3.338 | – |
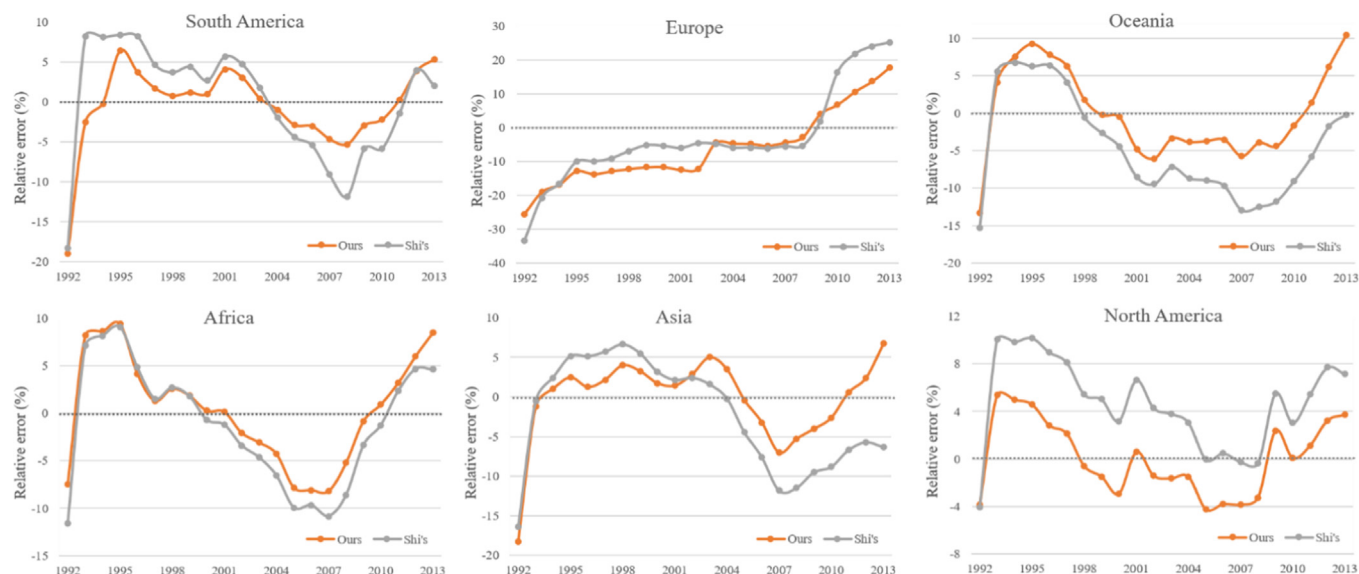


**Fig. 6.** Comparison for each year in 1992–2013 between Shi's product and ours at the continental level. The dashed line in each subfigure indicates the RE of zero.

**Table 6**
Comparison of the accuracy at the continental level.

| MARE (%) | South America | Europe | Oceania | Africa | Asia | North America |
|---|---|---|---|---|---|---|
| Shi's | 5.939 | 11.417 | 7.220 | 5.394 | 5.872 | 5.125 |
| Ours | 3.450 | 10.927 | 5.005 | 4.638 | 3.658 | 2.711 |

**Table 7**
Criteria of the MARE values for model evaluation.

| MARE | Evaluation |
|---|---|
| MARE ≤ 10% | High-accuracy estimation |
| 10% < MARE ≤ 20% | Good estimation |
| 20% < MARE ≤ 50% | Reasonable estimation |
| MARE > 50% | Inaccurate estimation |

be found in North America, South America, Oceania, and Asia when the *p*-value was set to 0.1 in the ANOVA test, implying that our method achieves a noticeable improvement.

### 5.1.3. Comparison at the national level

According to the MARE criteria for model evaluation (Table 7) [56,60], we calculated the number of countries/districts in each accuracy level for the two products. Since the spatial resolution of both products is 1 km, countries/districts with an area of less than 2 pixels were excluded from the comparison. From Fig. 7, it can be clearly observed that the estimation in most countries/districts (57.8%) achieved by our method shows a high accuracy, which is much better than that of Shi's product (17.8%). The percentage of countries with a good accuracy in our product is 27.4%, which is also higher than that of Shi's
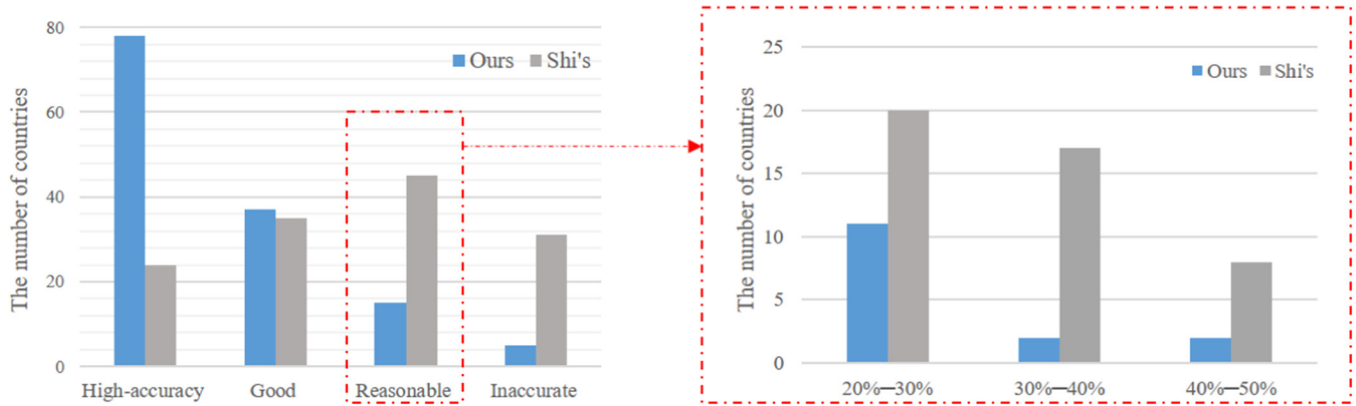
Fig. 7. Comparison of the accuracy between Shi's Product and ours.

product (25.9%). In addition, the countries with inaccurate estimation account for only 3.7% in our product, which is significantly less than the 23.0% in Shi's product. Furthermore, the range of reasonable estimation is further subdivided with the step of 10% (Fig. 7). In general, it can be concluded that the proposed locally adaptive method achieves a considerable improvement at the national-scale comparison.

The five countries with inaccurate estimation in our method are Estonia, Finland, Iceland, Norway, and Mozambique. The first four countries are all located in high-latitude zones, where the DMSP-OLS NSL data quality can be largely degraded by heavier cloud coverage and longer summer days (the acquisition time of DMSP-OLS is from 7p.m. to 9p.m. local time) [38,61]. This is a possible reason why the accuracies of these countries are relatively poor. Fig. 8 displays the annual EPC statistics for Mozambique during 1992–2013. All the candidate models are not well suited to fit this S-like curve, leading to an unsatisfactory MARE value for the EPC estimation. A piecewise function is a potential way to tackle this problem, which will be investigated in the future research.

### 5.2. Spatiotemporal analysis of EPC during 1992–2013

A positive value of global Moran's I indicates positive spatial autocorrelation. The higher the positive value, the more obvious the spatial autocorrelation. As Fig. 9 shows, there were significant positive spatial autocorrelations of provincial/state-level EPC in the world, as well as in each continent, from 1992 to 2013. At the global scale, the value of global Moran's I showed a relatively stable status from 1992 to 2010, and then increased from 0.5642 in 2010 to 0.6141 in 2013. In terms of the continental scale, the degree of spatial autocorrelation in Oceania and North America was higher than that in the other four continents. The degree of spatial autocorrelation in Oceania generally decreased
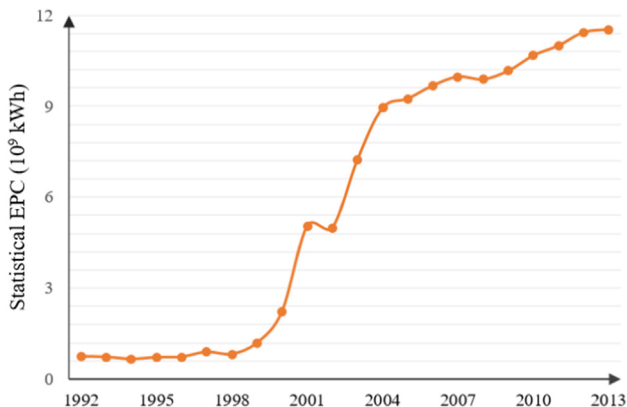


Fig. 8. Statistical EPC values in Mozambique during 1992–2013.

from 1992 to 2013, while that in North America presented a relatively steady tendency. With respect to the temporal change of global Moran's I, Asia witnessed more growth than the other continents, i.e., 0.4664 in 1992, increasing to 0.6189 in 2013. The global Moran's I in South America increased from 0.3882 to 0.4763, whereas the index in Africa changed from 0.3115 to 0.4102 over these 22 years. The degree of spatial autocorrelation in Europe first went up, and then declined during the study period.

We further calculated the global Moran's I in the United States, China, and India (Fig. 10), based on the aggregated EPC of the Level 2 subdivision unit in GADM. For instance, the Level-2 subdivision unit of GADM in China is the prefectural level. These three countries were selected as representatives due to their different urbanization and industrialization levels. It can be seen that the global Moran's I in China increased sharply from 0.2909 in 1992 to 0.4349 in 2013, which is probably related to the rapid urbanization during these 22 years. The global Moran's I of India also showed an upward trend from 1992 to 2013, whereas the change of global Moran's I in the United States was not as obvious as for the other two countries.

Subsequently, local Moran's I indices of all the provinces/states in 1992 and 2013 were calculated to analyze the spatial clustering patterns across the world (Fig. 11). The High-High cluster indicates spatial clustering of high EPC values. In contrast, the Low-Low cluster type reveals concentrations of low EPC values. During the study period, provinces/states with the High-High cluster type can be found in North America, Europe, and Asia, while the Low-Low spatial cluster mainly appears in Africa, North Europe, and Southeast Asia. The most notable change of EPC in the High-High cluster from 1992 to 2013 occurred in China, Russia, and India, indicating the significant increase of EPC in these three countries. The Low-High cluster means that a province/state with low EPC is encompassed by ones with high EPC. The provinces/states that were newly marked as this type mainly appeared in Mongolia, Kazakhstan, and Canada, which can possibly be ascribed to the huge EPC levels in neighboring countries, i.e., China and the United States.

Fig. 12 displays the temporal variation types of the provincial/state-level EPC in the world, according to the SLOPE index. The provinces/states belonging to the rapid growth type are located in the eastern coastal regions of China. The regions that experienced relatively rapid growth are mainly concentrated in China, the United States, and Russia. The moderate growth type mainly occurs in some provinces/states in China, India, Brazil, the United States, and Australia. Except for Brazil, other countries in South America show a relatively slow to slow growth. The major growth types in Europe are the relatively slow and slow types. Most of the provinces/states in Africa witnessed slow growth during the period.
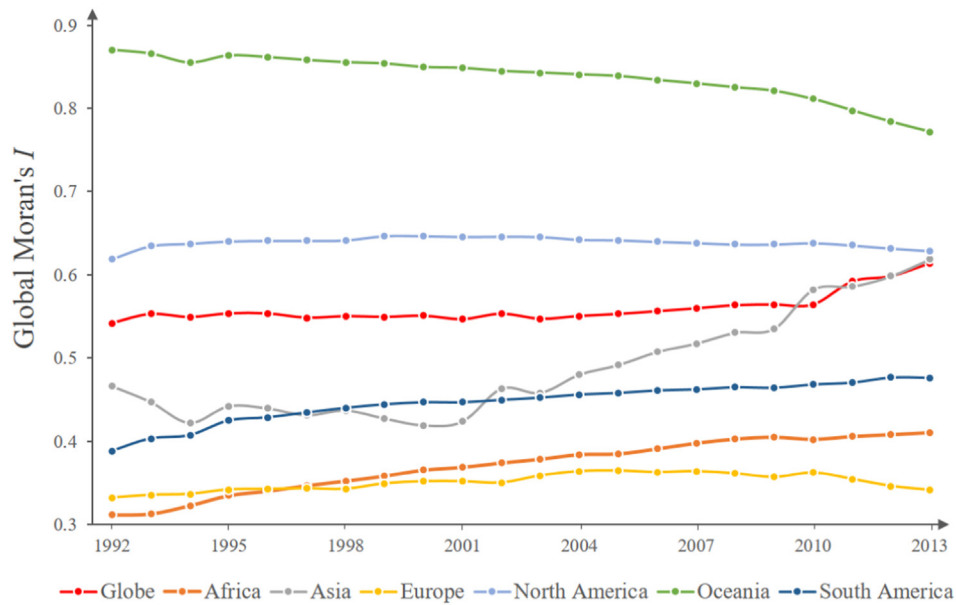
**Fig. 9.** Annual change of global Moran's *I* values for provincial/state-level EPC at global and continental scales.
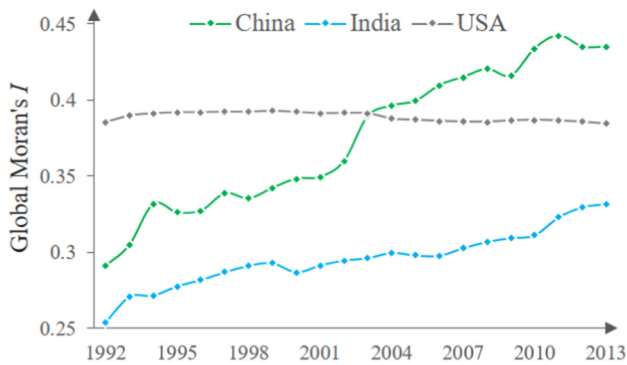


**Fig. 10.** Annual change of global Moran's *I* values for prefectural-level EPC in China, India, and USA.

### 5.3. Correlations with other socio-economic variables

In order to investigate the correlations between EPC and other socio-economic variables at the grid scale, three global gridded datasets, i.e., the Gridded Population of the World version 4 (GPWv4) [62], and the Global Land Cover 2000 (GLC2000) [63], and the total Gross Domestic Product (GDP) [64] in 2000 are adopted to represent different perspectives of socioeconomic types. All the three products are about 1 km resolution at the equator. The GLC2000 dataset is utilized to indicate the built-up area (BUA), and the pixels with the label of artificial surfaces and associated areas are regarded as built-up. Specifically, the world is partitioned into 6 EPC grades according to the division of gridded map of 2000 in Fig. 5. In this way, different regions in the same country may belong to different grades. Suppose $G_i$ denotes the *i*th EPC grade, and $N_i$ countries/districts are involved in this grade. In each EPC grade, $N_i$ points are obtained using the sum of EPC and the sum of BUA (or POP/GDP) of all the pixels within each country, and the correlation coefficients ($\rho$) are then measured. From Fig. 13, it can be seen that the correlation coefficients ($\rho$) for all the three socio-economic variables generally increases as the EPC grades rise. In particular, in the grade of high EPC ($> 5000$ MWh), the values of $\rho$ are above 0.83 for all the variables. In addition, compared to BUA and POP, GDP shows closer relationship with EPC in various EPC levels in terms of their correlation coefficients.

### 6. Conclusion

The DMSP-OLS nighttime stable light (NSL) images have the ability to model gridded electricity power consumption (EPC) across the globe. However, we need to properly deal with the saturation problem, as well as the incomparability and discontinuity issues existing in the original NSL data, to make the data a reasonable approximation of EPC. The regression model can then be built to quantify the relationship between the EPC statistics and the corrected NSL for the gridded EPC estimation. However, the previous research on global EPC estimation did not sufficiently consider the local socioeconomic differences among countries/districts in the NSL data correction and model establishment. Therefore, we have made improvements to the current product in the following aspects:

(1) Saturation in the NSL data is not a universal phenomenon over the world. Unnecessary saturation correction would cause distortion to the unsaturated pixels, e.g., in undeveloped areas. Therefore, we set up two options (i.e., with or without the saturation correction) and adaptively determine the saturation correction approach.
(2) The inter-annual correction is utilized to remove the discontinuity effect of time-series NSL data. Nevertheless, the different correction directions are preferred for different local areas due to the differences in the socioeconomic dynamics. Therefore, we provide three options (i.e., forward, backward, or average) in the correction direction in the proposed model.
(3) The relationship between EPC and corrected NSL is largely affected by the local socioeconomic status. Therefore, we set up four options in the selection of the regression model (i.e., linear, logarithmic, exponential, and second-order polynomial functions), to cope with the issue of diverse socioeconomic patterns around the world.

The core idea of our method is to adaptively select the optimal combinations from all the possible options for EPC modeling. The proposed method represents a novel attempt to adopt locally adaptive selection of the optimal processing chain for modeling global EPC.

The proposed method was utilized to construct 1-km global EPC maps from 1992 to 2013. Compared with the existing global product [44], the maps we generated are superior at global, continental, and national levels. In particular, the percentage of countries/districts in the high-accuracy level increases dramatically from 17.8% to 57.8%, while
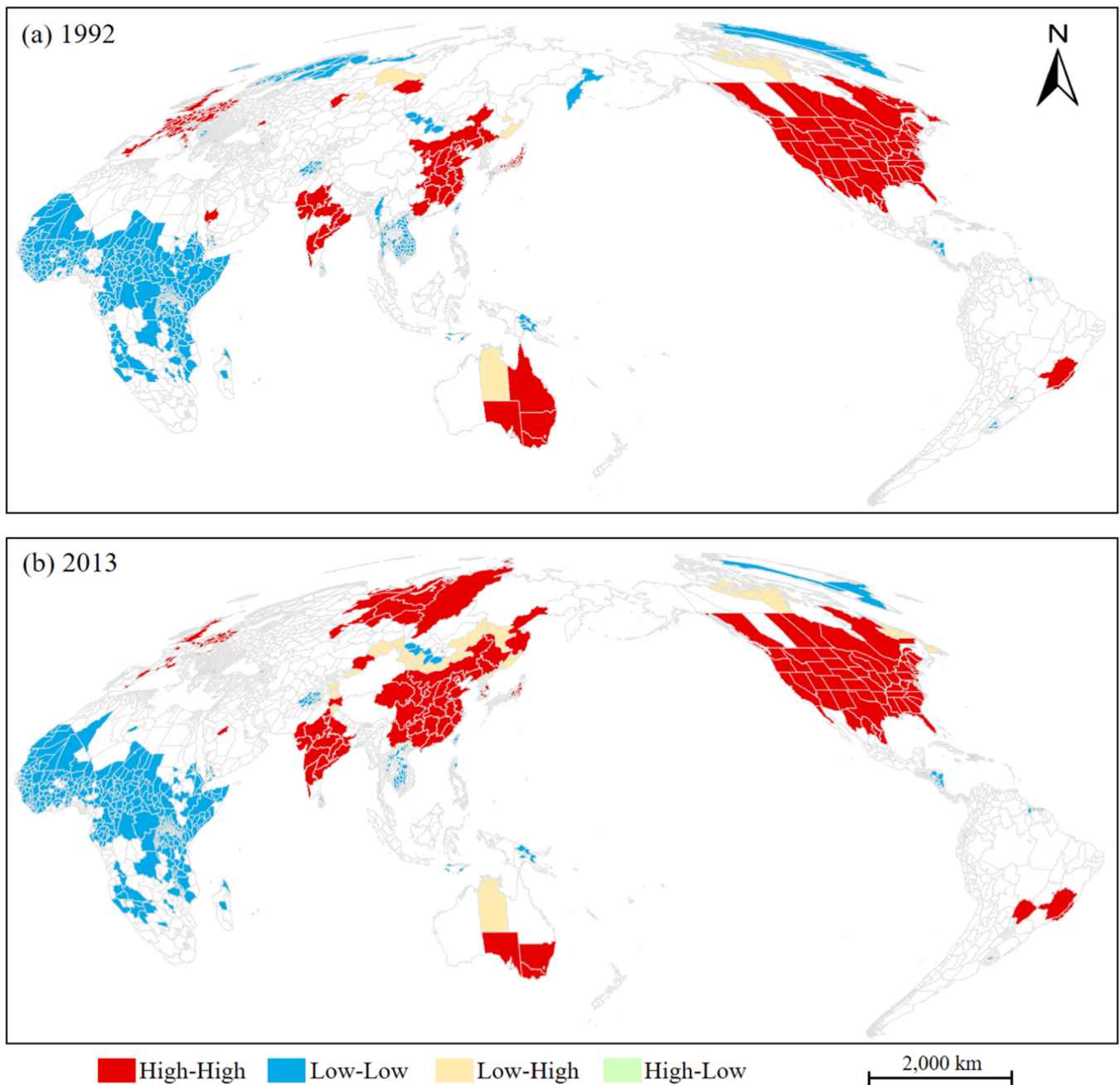
**Fig. 11.** Spatial clustering of neighborhood provinces/states in: (a) 1992 and (b) 2013 at the global scale.

the proportion of countries/districts in the inaccurate level drops from 23.0% to 3.7%. It can be concluded that the proposed locally adaptive approach to modeling global EPC is both reasonable and effective. The spatiotemporal dynamics of EPC were further analyzed based on the aggregated provincial/state-level EPC. The degree of spatial auto-correlation (i.e., global Moran's *I*) showed an upward trend from 1992 to 2013 at the global scale, signifying that the patterns of provincial/state-level EPC have become more clustered. At the continental scale, the degree of spatial clustering in Asia, South America, and Africa experienced more growth than the other continents. With respect to the cluster pattern of the local Moran's *I* index, provinces/states with a high EPC were mostly located in North America, Europe, and Asia. China witnessed moderate to fast growth of EPC. In addition, the United States, Russia, Brazil, and India also experienced moderate EPC growth during the study period.

Our product can be further analyzed with other spatial data layers.

For instance, the correlations between EPC and other socio-economic variables (i.e., population count (POP), built-up area (BUA), and gross domestic product (GDP)) were explored. It was revealed that the correlation between EPC and BUA/POP/GDP becomes closer as the EPC grade rises. It was also found that GDP is more relevant to EPC, compared to population and built-up area.

The proposed locally adaptive method could also be applied to other global products related to nighttime light data, such as carbon dioxide emission. In addition, the accuracy of our product could be further improved when more regression models or more statistical data are used to quantify the relationship between NSL and EPC, such as piecewise function [65] and machine learning methods. Moreover, with the release of the global Suomi National Polar-orbiting Partnership (NPP) Visible Infrared Imaging Radiometer Suite (VIIRS) nighttime light data [66–68], it should be possible to produce global EPC maps at a 500-m resolution. As a result, it should also be possible to monitor the
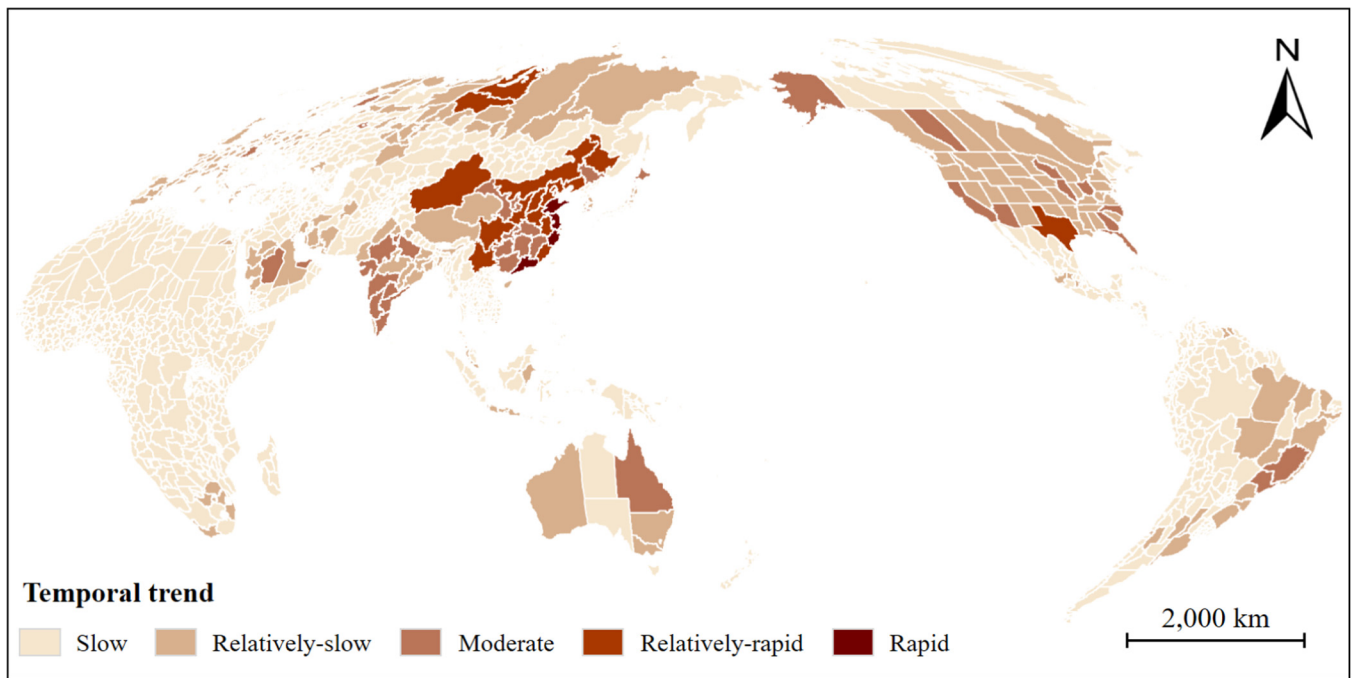
**Fig. 12.** Temporal variation types of the provincial/state-level EPC at the global scale from 1992 to 2013.
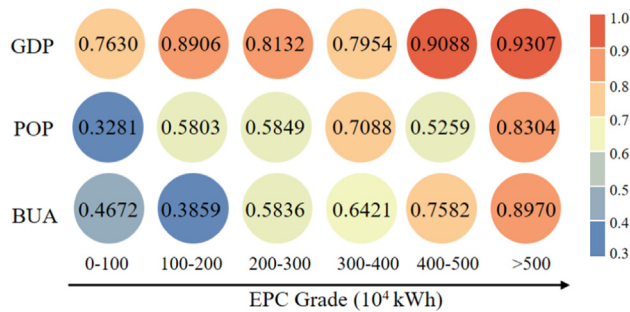


**Fig. 13.** Correlation coefficients between EPC and socio-economic variables for different EPC grades. POP: population count.

spatiotemporal dynamics at a finer resolution.

## Acknowledgements

## References

[1] Jacobson MZ. Review of solutions to global warming, air pollution, and energy security. Energy Environ Sci 2009;2:148–73.

[2] Chang C-C. A multivariate causality test of carbon dioxide emissions, energy consumption and economic growth in China. Appl Energy 2010;87:3533–7.

[3] Liu L, Sun X, Chen C, Zhao E. How will auctioning impact on the carbon emission abatement cost of electric power generation sector in China? Appl Energy 2016;168:594–609.

[4] Al-mulali U, Sab CNBC, Fereidouni HG. Exploring the bi-directional long run relationship between urbanization, energy consumption, and carbon dioxide emission. Energy 2012;46:156–67.

[5] Mahalingam B, Orman WH. GDP and energy consumption: A panel analysis of the US. Appl Energy 2018;213:208–18.

[6] The World Bank. World Development Indicators (WDI); 2018. https://data.worldbank.org/.

[7] Parshall L, Gurney K, Hammer SA, Mendoza D, Zhou Y, Geethakumar S. Modeling energy consumption and CO2 emissions at the urban scale: Methodological challenges and insights from the United States. Energy Policy 2010;38:4765–82.

[8] Wang S, Liu X, Zhou C, Hu J, Ou J. Examining the impacts of socioeconomic factors, urban form, and transportation networks on $CO_2$ emissions in China's megacities. Appl Energy 2017;185:189–200.

[9] Lean HH, Smyth R. $CO_2$ emissions, electricity consumption and output in ASEAN. Appl Energy 2010;87:1858–64.

[10] Abosedra S, Dah A, Ghosh S. Electricity consumption and economic growth, the case of Lebanon. Appl Energy 2009;86:429–32.

[11] Al-Garni AZ, Zubair SM, Nizami JS. A regression model for electric-energy-consumption forecasting in Eastern Saudi Arabia. Energy 1994;19:1043–9.

[12] Egelioglu F, Mohamad AA, Guven H. Economic variables and electricity consumption in Northern Cyprus. Energy 2001;26:355–62.

[13] Shiu A, Lam P-L. Electricity consumption and economic growth in China. Energy Policy 2004;32:47–54.

[14] Huang M, He Y, Cen H. Predictive analysis on electric-power supply and demand in China. Renew Energy 2007;32:1165–74.

[15] Chujai P, Kerdprasop N, Kerdprasop K. Time series analysis of household electric consumption with ARIMA and ARMA models. Proceedings of the international multiconference of engineers and computer scientists, vol. 1. 2013. p. 295–300.

[16] de Assis Cabral J, Legey LFL, de Freitas Cabral MV. Electricity consumption forecasting in Brazil: A spatial econometrics approach. Energy 2017;126:124–31.

[17] Huang W, Ma D, Chen W. Connecting water and energy: Assessing the impacts of carbon and water constraints on China's power sector. Appl Energy 2017;185:1497–505.

[18] Shi K, Yu B, Huang Y, Hu Y, Yin B, Chen Z, et al. Evaluating the ability of NPP-VIIRS nighttime light data to estimate the gross domestic product and the electric power consumption of China at multiple scales: A comparison with DMSP-OLS data. Remote Sens 2014;6:1705–24.

[19] Qin J, Chen Z, Yang K, Liang S, Tang W. Estimation of monthly-mean daily global solar radiation based on MODIS and TRMM products. Appl Energy 2011;88:2480–9.

[20] Fu P, Weng Q. A time series analysis of urbanization induced land use and land cover change and its impact on land surface temperature with Landsat imagery. Remote Sens Environ 2016;175:205–14.

[21] Huang X, Wen D, Li J, Qin R. Multi-level monitoring of subtle urban changes for the megacities of china using high-resolution multi-view satellite imagery. Remote Sens Environ 2017;196:56–75.

[22] Shi K, Chen Y, Li L, Huang C. Spatiotemporal variations of urban $CO_2$ emissions in China: A multiscale perspective. Appl Energy 2018;211:218–29.

[23] Letu H, Hara M, Tana G, Bao Y, Nishio F. Generating the nighttime light of the human settlements by identifying periodic components from DMSP/OLS satellite imagery. Environ Sci Technol 2015;49:10503–9.

[24] Jing X, Shao X, Cao C, Fu X. Comparison between DMSP-OLS and S-NPP day-night band in correlating with regional socio-economic variables. AGU Fall Meeting Abstracts; 2013.

[25] Shi K, Yu B, Zhou Y, Chen Y, Yang C, Chen Z, et al. Spatiotemporal variations of $CO_2$ emissions and their impact factors in China: A comparative analysis between the provincial and prefectural levels. Appl Energy 2019;233:170–81.

[26] Lu H, Liu G. Spatial effects of carbon dioxide emissions from residential energy consumption: A county-level study using enhanced nocturnal lighting. Appl Energy

2014;131:297–306.

[27] Xiao H, Ma Z, Mi Z, Kelsey J, Zheng J, Yin W, et al. Spatio-temporal simulation of energy consumption in China's provinces based on satellite night-time light data. Appl Energy 2018;231:1070–8.

[28] Elvidge CD, Imhoff ML, Baugh KE, Hobson VR, Nelson I, Safran J, et al. Night-time lights of the world: 1994–1995. ISPRS J Photogram Remote Sens 2001;56:81–99.

[29] Lo C. Urban indicators of china from radiance-calibrated digital DMSP-OLS night-time images. Ann Assoc Am Geogr 2002;92:225–40.

[30] Amaral S, Câmara G, Monteiro AMV, Quintanilha JA, Elvidge CD. Estimating population and energy consumption in Brazilian Amazonia using DMSP night-time satellite data. Comput Environ Urban Syst 2005;29:179–95.

[31] Chand TK, Badarinath K, Elvidge C, Tuttle B. Spatial characterization of electrical power consumption patterns over India using temporal DMSP-OLS night-time satellite data. Int J Remote Sens 2009;30:647–61.

[32] Townsend AC, Bruce DA. The use of night-time lights satellite imagery as a measure of Australia's regional electricity consumption and population distribution. Int J Remote Sens 2010;31:4459–80.

[33] Letu H, Hara M, Yagi H, Naoki K, Tana G, Nishio F, et al. Estimating energy consumption from night-time DMPS/OLS imagery after correcting for saturation effects. Int J Remote Sens 2010;31:4443–58.

[34] Letu H, Hara M, Tana G, Nishio F. A saturated light correction method for DMSP/OLS nighttime satellite imagery. IEEE Trans Geosci Remote Sens 2012;50:389–96.

[35] He C, Ma Q, Li T, Yang Y, Liu Z. Spatiotemporal dynamics of electric power consumption in Chinese Mainland from 1995 to 2008 modeled using DMSP/OLS stable nighttime lights data. J Geog Sci 2012;22:125–36.

[36] Ma T, Zhou C, Pei T, Haynie S, Fan J. Quantitative estimation of urbanization dynamics using time series of DMSP/OLS nighttime light data: A comparative case study from China's cities. Remote Sens Environ 2012;124:99–107.

[37] Xie Y, Weng Q. World energy consumption pattern as revealed by DMSP-OLS nighttime light imagery. GIScience & Remote Sens 2016;53:265–82.

[38] Jing X, Shao X, Cao C, Fu X, Yan L. Comparison between the Suomi-NPP Day-Night Band and DMSP-OLS for correlating socio-economic variables at the provincial level in China. Remote Sens 2016;8:17.

[39] Zhao N, Ghosh T, Samson EL. Mapping spatio-temporal changes of Chinese electric power consumption using night-time imagery. Int J Remote Sens 2012;33:6304–20.

[40] Cao X, Wang J, Chen J, Shi F. Spatialization of electricity consumption of China using saturation-corrected DMSP-OLS data. Int J Appl Earth Obs Geoinf 2014;28:193–200.

[41] He C, Ma Q, Liu Z, Zhang Q. Modeling the spatiotemporal dynamics of electric power consumption in Mainland China using saturation-corrected DMSP/OLS nighttime stable light data. Int J Digital Earth 2014;7:993–1014.

[42] Xie Y, Weng Q. Detecting urban-scale dynamics of electricity consumption at Chinese cities using time-series DMSP-OLS (Defense Meteorological Satellite Program-Operational Linescan System) nighttime light imageries. Energy 2016;100:177–89.

[43] Pan J, Li J. Spatiotemporal dynamics of electricity consumption in China. Appl Spat Anal Policy 2017:1–28.

[44] Shi K, Chen Y, Yu B, Xu T, Yang C, Li L, et al. Detecting spatiotemporal dynamics of global electric power consumption using DMSP-OLS nighttime stable light data. Appl Energy 2016;184:450–63.

[45] Elvidge CD, Baugh KE, Dietz JB, Bland T, Sutton PC, Kroehl HW. Radiance calibration of DMSP-OLS low-light imaging data of human settlements. Remote Sens Environ 1999;68:77–88.

[46] Wu J, Wang Z, Li W, Peng J. Exploring factors affecting the relationship between light consumption and GDP based on DMSP/OLS nighttime satellite imagery. Remote Sens Environ 2013;134:111–9.

[47] Wu J, He S, Peng J, Li W, Zhong X. Intercalibration of DMSP-OLS night-time light data by the invariant region method. Int J Remote Sens 2013;34:7356–68.

[48] Cao Z, Wu Z, Kuang Y, Huang N, Wang M. Coupling an intercalibration of radiance-calibrated nighttime light images and land use/cover data for modeling and analyzing the distribution of GDP in Guangdong, China. Sustainability 2016;8:108.

[49] Roy DP, Jin Y, Lewis P, Justice C. Prototyping a global algorithm for systematic fire-affected area mapping using MODIS time series data. Remote Sens Environ 2005;97:137–62.

[50] Dogan M, Ulke A, Cigizoglu HK. Trend direction changes of Turkish temperature series in the first half of 1990s. Theor Appl Climatol 2015;121:23–39.

[51] Zhang Q, Schaaf C, Seto KC. The vegetation adjusted NTL urban index: A new approach to reduce saturation and increase variation in nighttime luminosity. Remote Sens Environ 2013;129:32–41.

[52] Elvidge CD, Ziskin D, Baugh KE, Tuttle BT, Ghosh T, Pack DW, et al. A fifteen year record of global natural gas flaring derived from satellite data. Energies 2009;2:595–622.

[53] Meng L, Graus W, Worrell E, Huang B. Estimating $CO_2$ (carbon dioxide) emissions at urban scales by DMSP/OLS (Defense Meteorological Satellite Program's Operational Linescan System) nighttime light imagery: methodological challenges and a case study for China. Energy 2014;71:468–78.

[54] Letu H, Nakajima TY, Nishio F. Regional-scale estimation of electric power and power plant $CO_2$ emissions using defense meteorological satellite program operational linescan system nighttime satellite data. Environ Sci Technol Lett 2014;1:259–65.

[55] Shi K, Chen Y, Yu B, Xu T, Chen Z, Liu R, et al. Modeling spatiotemporal $CO_2$ (carbon dioxide) emission dynamics in China from DMSP-OLS nighttime stable light data using panel data analysis. Appl Energy 2016;168:523–33.

[56] Aydin G. Modeling of energy consumption based on economic and demographic factors: The case of Turkey with projections. Rene Sustain Energy Rev 2014;35:382–9.

[57] Ord JK. Spatial processes. Encyclopedia Statist Sci. 2004;12.

[58] Anselin L. Local indicators of spatial association—LISA. Geograph Anal 1995;27:93–115.

[59] Keselman H, Huberty CJ, Lix LM, Olejnik S, Cribbie RA, Donahue B, et al. Statistical practices of educational researchers: An analysis of their ANOVA, MANOVA, and ANCOVA analyses. Rev Edu Res 1998;68:350–86.

[60] Lewis CD. International and business forecasting methods. London: Butterworths; 1982.

[61] Zhang Q, Pandey B, Seto KC. A robust method to generate a consistent time series from DMSP/OLS nighttime light data. IEEE Trans Geosci Remote Sens 2016;54:5821–31.

[62] Center for International Earth Science Information Network (CIESIN)—Columbia University. Gridded Population of the World, Version 4 (GPWv4): Population Density. NASA Socioeconomic Data and Applications Center (SEDAC) Palisades, NY; 2016.

[63] Bartholome E, Belward AS. GLC2000: a new approach to global land cover mapping from Earth observation data. Int J Remote Sens 2005;26:1959–77.

[64] Kummu M, Taka M, Guillaume JH. Gridded global datasets for gross domestic product and Human Development Index over 1990–2015. Sci Data 2018;5.

[65] Hobbs BF, Pang J-S. Nash-Cournot equilibria in electric power markets with piecewise linear demand functions and joint constraints. Oper Res 2007;55:113–27.

[66] Cao C, Xiong J, Blonski S, Liu Q, Uprety S, Shao X, et al. Suomi NPP VIIRS sensor data record verification, validation, and long-term performance monitoring. J Geophys Res: Atmosph 2013;118:11,664–78.

[67] Shao X, Cao C, Zhang B, Qiu S, Elvidge C, Von Hendy M. Radiometric calibration of DMSP-OLS sensor using VIIRS day/night band. Earth Observing missions and sensors: development, implementation, and characterization III: international society for optics and photonics. 2014. p. 92640A.

[68] Zhao J, Ji G, Yue Y, Lai Z, Chen Y, Yang D, et al. Spatio-temporal dynamics of urban residential $CO_2$ emissions and their driving forces in China using the integrated two nighttime light datasets. Appl Energy 2019;235:612–24.